Journal of Magnetism and Magnetic Materials 554 (2022) 169316

Contents lists available at ScienceDirect

Journal of Magnetism and Magnetic Materials

journal homepage: www.elsevier.com/locate/jmmm

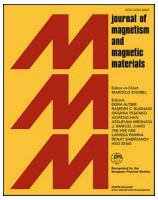

Magnetic domain configurations of pulsed laser deposited MnBi hard magnetic films

J. Vergara [a,b,*], C. Favieres [a,b], V. Madurga [a]

[a] Laboratory of Magnetism, Department of Science (Physics), Public University of Navarre, UPNA, Campus de Arrosadía, 31006 Pamplona, Spain
[b] Institute for Advanced Materials and Mathematics (INAMAT^2), Public University of Navarre, UPNA, Campus de Arrosadía, 31006 Pamplona, Spain

ARTICLE INFO

Keywords:
Rare-earth free permanent magnets
MnBi hard magnetic films
Magnetic domain configuration
Perpendicular anisotropy
Pulsed laser deposition

ABSTRACT

Hard magnetic MnBi films were obtained by appropriate heat treatments of pulsed laser deposited (PLD) (Bi/Mn) films. X-ray diffraction patterns indicated a slight texture of MnBi crystallites and magnetometry measurements showed a slight preferential growth of the crystallites with their c-axis perpendicular to the film plane. Magnetic force microscopy (MFM) measurements displayed the presence of magnetic domains, whose size was in the micrometer range, and which were correlated to the MnBi grains observed in the sample. The addition of extra Mn layers did not modify significantly the previous structural and magnetic results. Nevertheless, the size of the magnetic domains increased to a few microns. However, on adding extra Bi layers, upon annealing, the MnBi grains grew with their c-axes perpendicular to the film plane. A perpendicular to the film magnetic anisotropy was deduced from the hysteresis loops, where an increase in the remanence of the magnetization was measured when the magnetic field was applied perpendicular to the film plane. In these samples, by measuring the magnetic domain configuration of the samples by MFM, we observed that the size of the magnetic domains exceeded the dimensions of the grains. This change in the magnetic structure of the films was assumed to be due to the coupling of the magnetization in the neighboring grains, and it was responsible for the decrease of the coercivity in the Bi rich samples.

1. Introduction

MnBi has recently been demonstrated to be a good candidate to develop rare-earth-free permanent magnet materials. This compound may exhibit a value of its saturation magnetization ($\mu_0 M_S$) close to 0.7 T, a coercive field ($\mu_0 H_C$) well above 1 T and a Curie temperature on the order of 630 K that makes it quite appropriate for its use at elevated temperature [1,2]. MnBi, in its low temperature (LT) phase shows a rombohedral structure similar to NiAs which can be indexed in the $P6_3/mmc$ group. The magnetic moment in this MnBi alloy points along the c-axis of this crystalline structure [3].

MnBi hard magnetic films have been deposited by a wide variety of techniques, including sputtering [4–10], thermal and e-beam evaporation [11–13] and pulsed laser deposition [14–16]. The fabrication of these films as well as the study of their structural and magnetic properties can provide a useful insight for the further development of bulk permanent magnets.

In order to improve the hard magnetic property of MnBi compounds, previous works in the literature detailed the procedures to enhance the maximum BH product of the compound through different methods. For instance, heat treatments in the presence of magnetic fields gave rise to the orientation of the MnBi crystallites originating an alignment of the easy magnetization axes in the different grains [12]. Also, the addition of ferromagnetic layers with high saturation magnetization, that were coupled to the MnBi structure through exchange coupling, originated an increase in the total saturation magnetization of the system [17–21]. Furthermore, the control of the orientation of the MnBi crystallites through the deposition of Bi buffer layers has been used to tailor the magnetic properties of the MnBi compounds [14,15,22,23] although in different geometries, compared to the ones in this particular work.

In this framework, we fabricated MnBi films by laser deposition and we changed the environment of the MnBi grains by adding extra layers of either Mn or Bi. Particularly, for the films with extra Bi layers, showing an orientation of their c-axes perpendicular to the film plane, their hard magnetic property changed considerably. A correlation between the changes in the magnetic domain configurations of the MnBi films with extra Bi layers and the modifications in their magnetic properties was shown throughout this work.

* Corresponding author.
E-mail address: jvergara@unavarra.es (J. Vergara).

https://doi.org/10.1016/j.jmmm.2022.169316
Received 21 December 2021; Received in revised form 18 March 2022; Accepted 27 March 2022
Available online 30 March 2022

2. Experimental

PLD films were fabricated with a laser whose energy per pulse was 350 mJ, at a frequency of 20 Hz and with a pulse duration of 6 ns and a wavelength of 1064 nm. The deposition of the films took place at a typical pressure of 10^{-5} mbar. Particular details of the deposition technique were described in a previous work [24].

The samples were built by alternatively depositing Bi and Mn. Bi was deposited for ten seconds with an average deposition rate of 19 nm/min. Subsequently, Mn was laser deposited for twenty seconds with an average deposition rate of 4.2 nm/min. In these samples the relative concentration of Bi with respect to Mn was relative larger than the one measured in similar samples described in a previous work [16]. This basic deposition structure $Bi_{3.2nm}Mn_{1.4nm}$ was repeated 40 times in every sample, and it was particularly chosen since, after appropriate heat treatments, the LT α-MnBi phase was originated in the films. The atomic composition of the previous $(Bi_{3.2nm}Mn_{1.4nm})_{40}$ film was $(Bi_{0.45}Mn_{0.55})$. The atomic composition of some of the films was determined with the microanalysis probe of a JEOL JSM-5610 LV Scanning Electron Microscope. In some samples, we also added a 20 nm thick (in average) Mn buffer layer as well as a 20 nm (in average) thick Mn capping layer to the basic 40 (Bi/Mn) structure. And in other samples, to the basic (Bi/Mn) building block, we added both a 50 nm thick (in average) Bi buffer layer and a 50 nm (in average) thick Bi capping layer. In all the samples, a 15 nm (in average) thick Ta protective layer was deposited to avoid oxidation. For all these samples, the distance between the target and the glass substrates was 85 mm.

As indicated above, annealing processes on every sample were

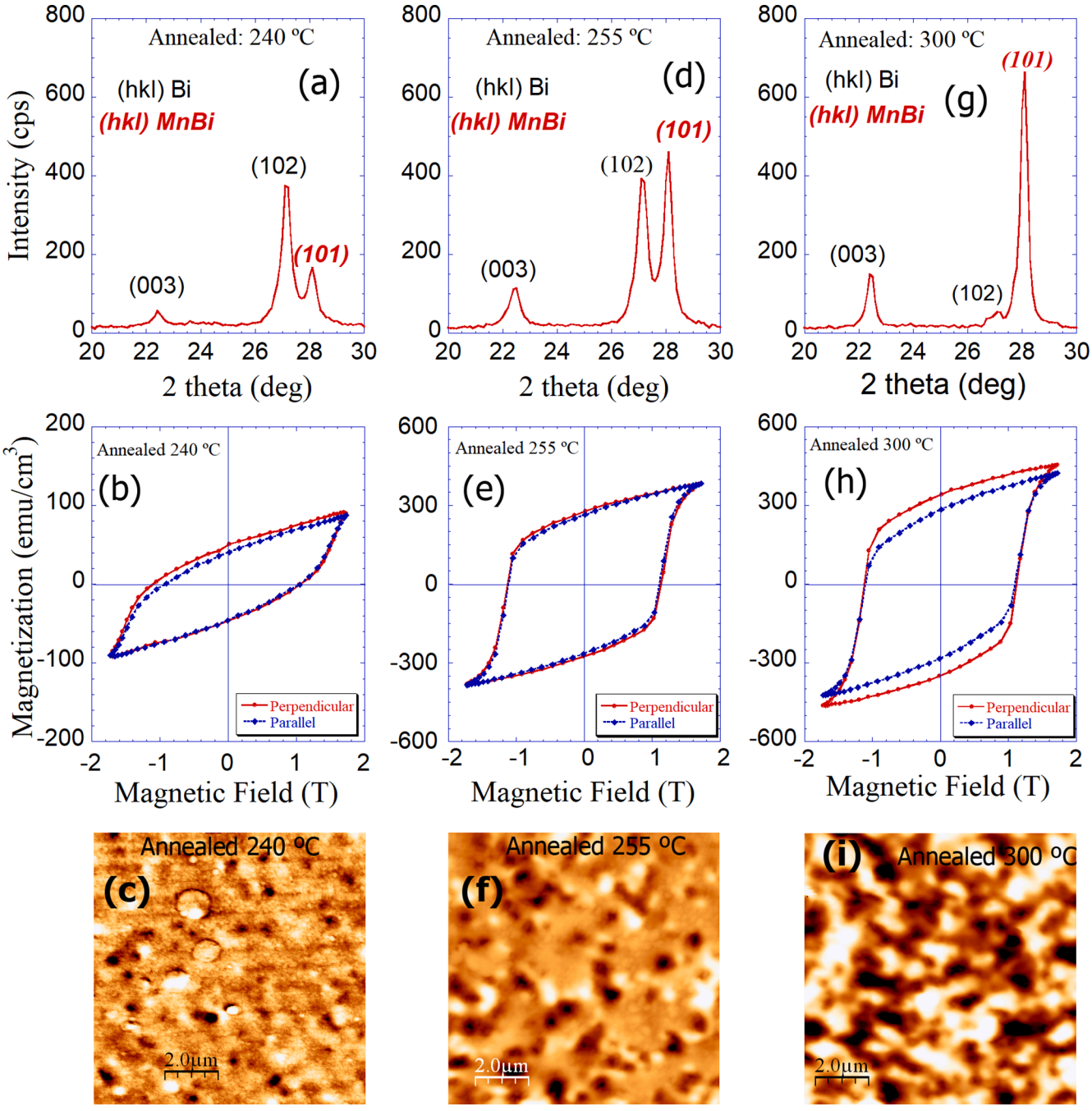

Fig. 1. X-ray diffraction patterns (a), (d), (g), room temperature magnetic hysteresis loops (b), (e), (h) and MFM images (c), (f), (i) of the $(Bi_{3.2nm}Mn_{1.4nm})_{40}/Ta_{15nm}$ films that were annealed respectively at 240, 255 and 300 °C. (Notice that the vertical scales in figures (b), (e) and (h) are different).

performed ex-situ in a homemade furnace in a dynamic Ar atmosphere. The temperature increased at a rate of 9 K/min until the annealing temperature, that was kept for 2 min. The decreasing rate was 9 K/min too.

X-ray diffraction patterns on the different samples were measured with a Seifert XRD3000 diffractometer using the Cu K-α radiation in the θ-2θ geometry. Rocking curve measurements, changing the omega angle, around particular diffraction peaks were also performed.

The room temperature hysteresis loops of the samples were measured with an EG&G vibrating sample magnetometer (VSM) at room temperature and in magnetic fields up to 1.7 T.

The surface morphology of the samples and the magnetic configuration at the microscopic scale were measured with a Nanotec atomic/magnetic force microscope (AFM/MFM) [25] and with commercial MESP tips from Veeco coated with a CoCr layer. The thickness of the films was also measured by AFM and the previously mentioned values of the deposition rates were extracted from these measurements. The MFM images in these hard magnetic films corresponded to the magnetic domain configurations [26]. The contrast in the scale in the different MFM images was normalized. In this way, a direct comparison of the interaction of the MFM tip and the different samples could be established.

3. Results

3.1. $(Bi_{3.2nm}Mn_{1.4nm})_{40}$ film

The films were initially annealed to 240 °C. The X-ray diffraction pattern of the sample, cf. Fig. 1(a), revealed the presence of an incipient polycristalline MnBi phase through the presence of the (1 0 1) diffraction peak of MnBi, as well as the presence of pure Bi that had not been combined with Mn after annealing at 240 °C. No peaks corresponding to pure Mn were observed in the X-ray diffraction patterns, indicating that Mn could remain in the sample either in an amorphous or nanocrystalline phase. The magnetic hysteresis loops of this sample, with the applied magnetic field either in the plane of the sample or perpendicular to it, are represented in Fig. 1(b). The value of the measured magnetization in the sample was relatively small, compared to the value of bulk MnBi. This particular magnetization was originated by MnBi particles as shown in the MFM image of the demagnetized sample, represented in Fig. 1(c). The estimated average size of the MnBi particles in this sample was around 500 nm, from the MFM measurements.

On annealing the sample at a higher temperature, 255 °C, the volume of the MnBi phase was enhanced in the sample. Thus, the intensity of the (1 0 1) characteristic peak of the MnBi phase also increased, cf. Fig. 1(d). The magnetization of the sample annealed at 255 °C, cf. Fig. 1(e) increased too, both when the magnetic field was applied along the in plane or along the perpendicular to the film plane direction. The isotropic behaviour of the magnetization indicated that the c-axis of the MnBi grains, i.e. the directions where the magnetization pointed, were randomly distributed in the sample. The 10x10 μm^2 MFM image of the demagnetized 255 °C annealed sample, cf. Fig. 1(f) showed the presence of MnBi magnetic domains whose size was approximately in the range of 800 nm.

When the annealing temperature rose to 300 °C, the volume of MnBi phase in our samples reached its maximum value, meanwhile the remaining amount of Bi was in its minimum value in the sample. Thus, cf. Fig. 1(g), the intensity of the characteristic (1 0 1) MnBi diffraction peak reached its highest value and the Bi (1 0 2) peak was almost negligible. Only a small fraction of Bi remained in the sample, oriented in such a way that the Bi grains grew with the c-axis of the Bi hexagonal structure perpendicular to the plane of the sample. In Fig. 1(h), the magnetization of the sample increased to 450 emu/cm^3 at room temperature and for an applied magnetic field of 1.7 Tesla perpendicular to the film plane. When the applied magnetic field was in the plane of the sample, the magnetization reached a smaller value, around 425 emu/cm^3. A slight preferential orientation of the magnetization of the sample along the perpendicular direction could inferred from the room temperature magnetization isotherms. The 10x10 μm^2 MFM image of the 300 °C annealed sample, cf. Fig. 1(i) showed a magnetic domain configuration where the size of the magnetic domains was in the range of 1 μm. Heat treatments at tempertures slightly above 300 °C did not show considerable differences with respect to what was shown in Fig. 1 (g), 1(h) and 1(i). The volume fraction of the MnBi phase in the $(Bi_{3.2nm}Mn_{1.4nm})_{40}$ film sample was 80%. This estimation was obtained through the magnetic moment of the samples, measured by VSM and the volume of the samples, where their thicknesses were measured by AFM. The volume of the Ta protective layer was not taken into account.

3.2. $Mn_{20nm}/(Bi_{3.2nm}Mn_{1.4nm})_{40}/Mn_{20nm}$ film

The $Mn_{20nm}/(Bi_{3.2nm}Mn_{1.4nm})_{40}/Mn_{20nm}$ film was initially annealed at 240 °C, which for this sample, was the temperature of the onset of the formation of the MnBi phase, since an incipient maximum corresponding to the (1 0 1) diffraction peak of polycrystalline MnBi was observed in the X-ray diffraction pattern of the $Mn_{20nm}/(Bi_{3.2nm}Mn_{1.4nm})_{40}/Mn_{20nm}$ sample cf. Fig. 2(a), which was not previously observed after annealing the samples at lower temperatures. The (0 0 3) and (1 0 2) Bi diffraction peaks were also observed in that pattern. Again, no trace of Mn peaks were detected in the X-ray diffraction patterns, indicating again that the extra content of Mn might remain in the sample either in an amorphous or nanocrystalline state. The room temperature hysteresis loops of the sample, measured with the applied magnetic field both parallel and perpendicular to the film plane, are shown in Fig. 2(b). The MnBi particles that grew at 240 °C gave rise to an isotropic magnetic behavior. In Fig. 2(c) a 20 × 20 μm^2 MFM image is displayed. The presence of MnBi single magnetic domains whose size was on the order of 1 μm is evidenced in this image.

The film was subsequently annealed at 250 °C. The X-ray diffraction pattern of this sample is shown in Fig. 2(d). The characteristic (1 0 1) peak of the polycrystalline MnBi phase was observed, as well as the (1 0 2) maximum of the Bi phase, indicating that still not all the Bi had been alloyed with the Mn. The room temperature magnetic hysteresis loops corresponding to this sample are displayed in Fig. 2(e). Hysteresis loops with the applied magnetic field both in the film plane and also perpendicular to the film are displayed in the figure. A slight preferential orientation of the magnetization perpendicular to the film plane was observed and a maximum magnetization on the order of 400 emu/cm^3 was measured for the perpendicular configuration. The MFM image corresponding to this sample is displayed in Fig. 2(f). The size and the amount of magnetic domains increased in this sample, compared to the previous image. Consequently, in this temperature range, the increase in the annealing temperature seemed to promote the growth in number and in size of the MnBi grains, giving rise to an increase in the intensity of the MnBi diffraction peaks and of the magnetization of the sample.

On increasing the annealing temperature to 260 °C, the X-ray diffraction pattern of the sample, see Fig. 2(g), shows an increase in the intensity of the (1 0 1) MnBi peak, at the expense of the decrease of the (1 0 2) Bi diffraction maximum. This result confirmed that on increasing the annealing temperature the alloying process of Mn and Bi continued. Still a small amount of Bi remained unalloyed and its presence was manifested mainly in the (0 0 3) Bi peak. This result also indicates that this unalloyed Bi grew with its c-axis perpendicular to the film plane upon increasing the annealing temperature.

The room temperature hysteresis loops with the magnetic field applied along the in plane or perpendicular to the plane direction are shown in Fig. 2(h). The magnetization of the sample measured perpendicular to the film plane increased slightly, as well as the anisotropy in the magnetization. The presence of the Bi grains grown with their c-axis perpendicular to the film plane could promote this slight anisotropic behaviour that was not very different from what was observed in the MnBi samples without the Mn buffer and capping layers.

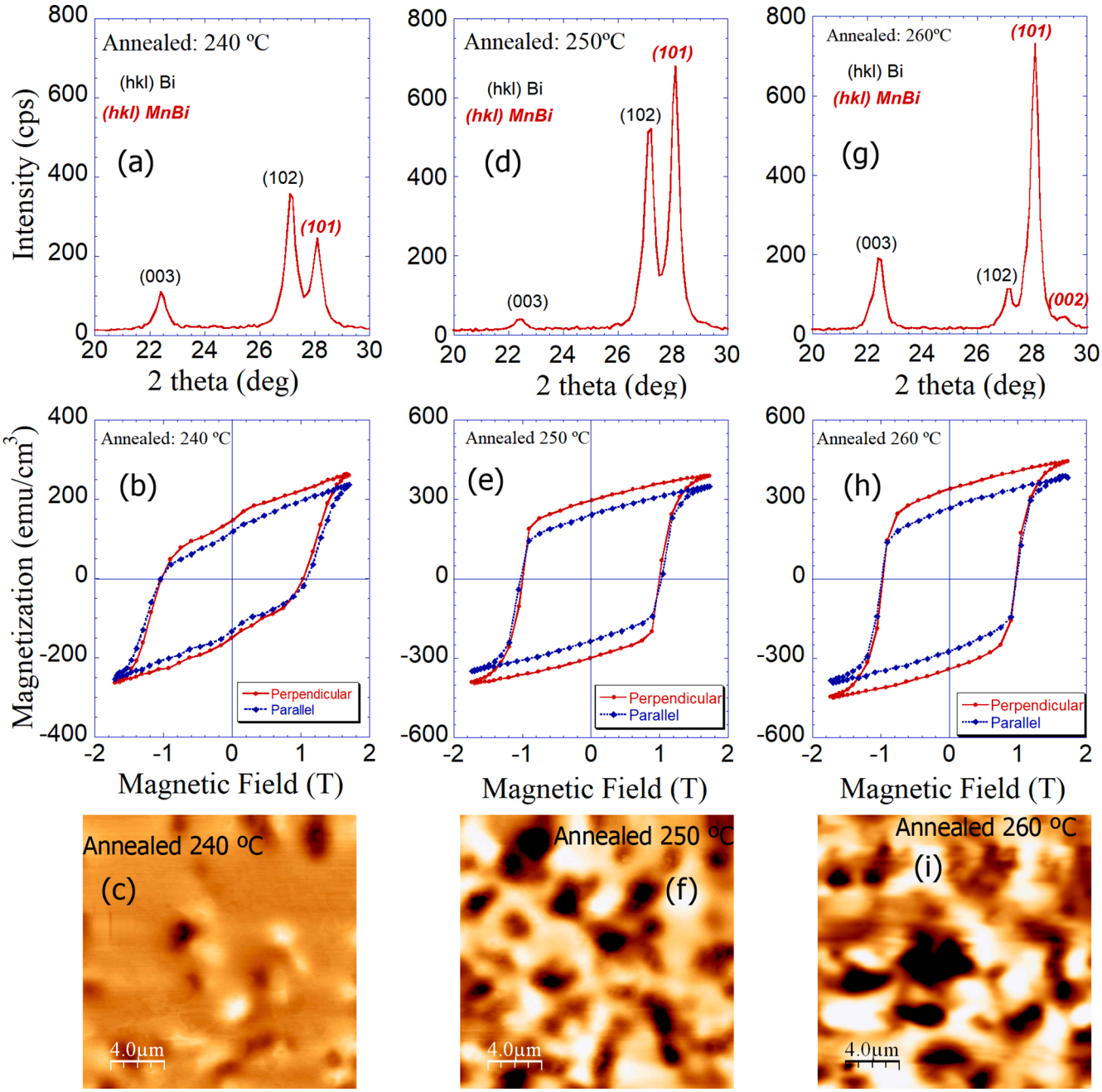

Fig. 2. X-ray diffraction patterns (a), (d), (g), room temperature magnetic hysteresis loops (b), (e), (h) and MFM images (c), (f), (i) of the $Mn_{20nm}/(Bi_{3.2nm}Mn_{1.4nm})_{40}/Mn_{20nm}$ films that were annealed respectively at 240, 250 and 260 °C. (Notice that the vertical scales in figures (b), (e) and (h) are different).

The corresponding MFM image for this sample is displayed in Fig. 2(i). As indicated above, the contrast in the different MFM images is the same. In this Fig. 2(i), definitely the number and the size of the magnetic domains (up to 4 μm) increased, with respect to the previous images from samples annealed at lower temperatures. In 2(i) the magnetic contrast occupies a larger amount of the image, which suggest that the MnBi phase was the prevailing phase in the sample. The volume fraction of the MnBi phase in $Mn_{20nm}/(Bi_{3.2nm}Mn_{1.4nm})_{40}/Mn_{20nm}$ film sample was 78%. The volume of the buffer and capping Mn layers as well as the volume of the Ta protective layer were not taken into account for this estimation.

When comparing the results of both the X-ray diffraction patterns and the magnetic hysteresis loops of the MnBi samples with or without Mn buffer and capping layers (from Figs. 1 and 2), no significant differences were found. So, this comparison indicated that the presence of an extra amount of Mn did not modify either the structure or the magnetic properties of the MnBi system. Just the increase in the size of the magnetic domains in the samples with extra Mn layers was the most significant change due to the addition of Mn.

3.3. $Bi_{50nm}/(Bi_{3.2nm}Mn_{1.4nm})_{40}/Bi_{50nm}$ film

The X-ray diffraction pattern of the $Bi_{50nm}/(Bi_{3.2nm}Mn_{1.4nm})_{40}/Bi_{50nm}$ sample annealed at 150 °C is represented in Fig. 3(a). At this annealing temperature an incipient MnBi phase was present. Still, a significant amount of Bi grown with their c-axis perpendicular to the deposition plane was present. Consequently, the (003) Bi diffraction peak showed a relatively high intensity. As indicated above, the presence of these preferentially oriented Bi grains promoted the formation of MnBi grains growing also with their c-axes perpendicular to the film

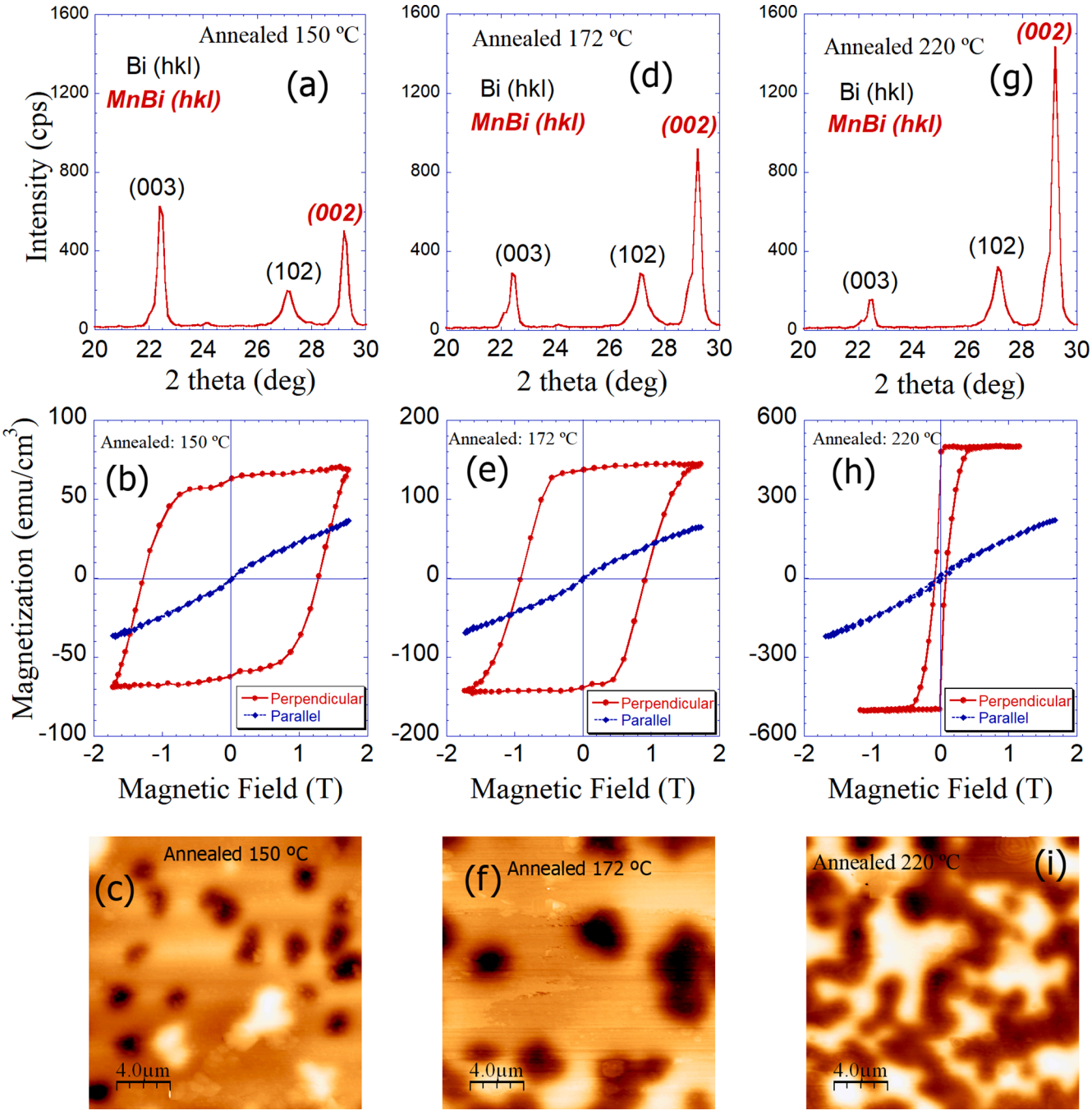

Fig. 3. X-ray diffraction patterns (a), (d), (g), room temperature magnetic hysteresis loops (b), (e), (h) and MFM images (c), (f), (i) of the $Bi_{50nm}/(Bi_{3.2nm}Mn_{1.4nm})_{40}/Bi_{50nm}$ films that were annealed respectively at 150, 172 and 220 °C. (Notice that the vertical scales in figures (b), (e) and (h) are different).

plane. In this way, for MnBi, only the (002) diffraction peak was observed and not the characteristic (101) peak of the polycrystalline MnBi. The room temperature magnetic hysteresis loops of the 150 °C annealed sample are shown in Fig. 3 (b). The main characteristic extracted from these magnetization isotherms was the existence of an easy magnetization direction perpendicular to the film plane. When the magnetic field was applied along the perpendicular direction, the hysteresis loop showed a remanence to saturation, M_r/M_S, ratio close to 1 and a coercive field ($\mu_0 H_c$) on the order of 1.35 T. On the other side, when the magnetic field was applied in the plane of the sample, an anhysteretic almost linear hysteresis loop was found. Fig. 3(c) displays a 20x20 μm^2 MFM image of the 150 °C annealed $Bi_{50nm}/(Bi_{3.2nm}Mn_{1.4nm})_{40}/Bi_{50nm}/Ta_{15nm}$ sample in the remanent state. The presence of individual MnBi magnetic domains whose size is on the order of 1 µm was evidenced through this image. In these MnBi single domains, according to the MFM image, the magnetization pointed perpendicular to the plane of the sample.

On annealing the $Bi_{50nm}/(Bi_{3.2nm}Mn_{1.4nm})_{40}/Bi_{50nm}$ sample to 172 °C, the corresponding X-ray diffraction pattern, cf. Fig. 3(d) showed similar features compared to the sample shown before. Again, the (003) Bi peak as well as the (002) MnBi maximum were observed. Also, a contribution of the characteristic (102) peak of the polycrystalline Bi was measured. However, the (101) peak of polycrystalline MnBi was not observed at all. Consequently, this result reinforced the previous assumption that the growth of the Bi crystallites perpendicular to the film plane promoted a similar growth in the MnBi crystallites. Room

temperature hysteresis loop of the 172 °C annealed sample are displayed in Fig. 3(e). These hysteresis loops confirm the existence of a perpendicular magnetic anisotropy as a consequence of the grain growth with the c-axis of the MnBi crystals perpendicular to the film plane. By extrapolation, the anisotropy field ($\mu_0 H_K$) of the sample would be approximately 3.5 T. For this 172 °C annealed, the value of the coercive field decreased to 1 Tesla. The 20x20 μm^2 MFM image of the 172 °C annealed Bi/(MnBi)/Bi sample is shown in Fig. 3(f). Again, MnBi single domains were observed in the image, but in this sample annealed at 172 °C, the average size of the domains had increased to 4 μm. Also, in this image, the high contrast observed in the MnBi domains indicated that the magnetization in these domains pointed perpendicular to the film plane.

The X-ray diffraction pattern of the $Bi_{50nm}/(Bi_{3.2nm}Mn_{1.4nm})_{40}/Bi_{50nm}$ sample annealed to 220 °C is displayed in Fig. 3 (g). The increase of the intensity of the (0 0 2) MnBi diffraction peak indicated a further growth of the MnBi phase in the sample. Again, this MnBi phase grew with the c-axis of its crystalline structure perpendicular to the film plane. No trace of the characteristic (1 0 1) diffraction peak of polycrystalline MnBi was detected. The magnetization of the 220 °C annealed sample also increased to 500 emu/cm^3, cf. the perpendicular hysteresis loop of Fig. 3(h). Again, the in-plane hysteresis loop was an almost linear anhysteretic curve indicating the presence of a perpendicular to the plane magnetic anisotropy, with extrapolated anisotropy field on the order of 3.5 T. In this sample, the coercive field in the perpendicular direction significantly decreased to 0.1 Tesla. The 20x20 μm^2 MFM image of the 220 °C annealed Bi/(MnBi)/Bi sample is shown in Fig. 3(i). As the MnBi phase continued growing in the film, as annealing temperatures increased, a multidomain magnetic structure was observed in the MFM image. It seems plausible that on increasing the volume of the MnBi phase, a coalescence of the MnBi domains took place, leading to the observed multidomain structure. Thus, the reversal of the

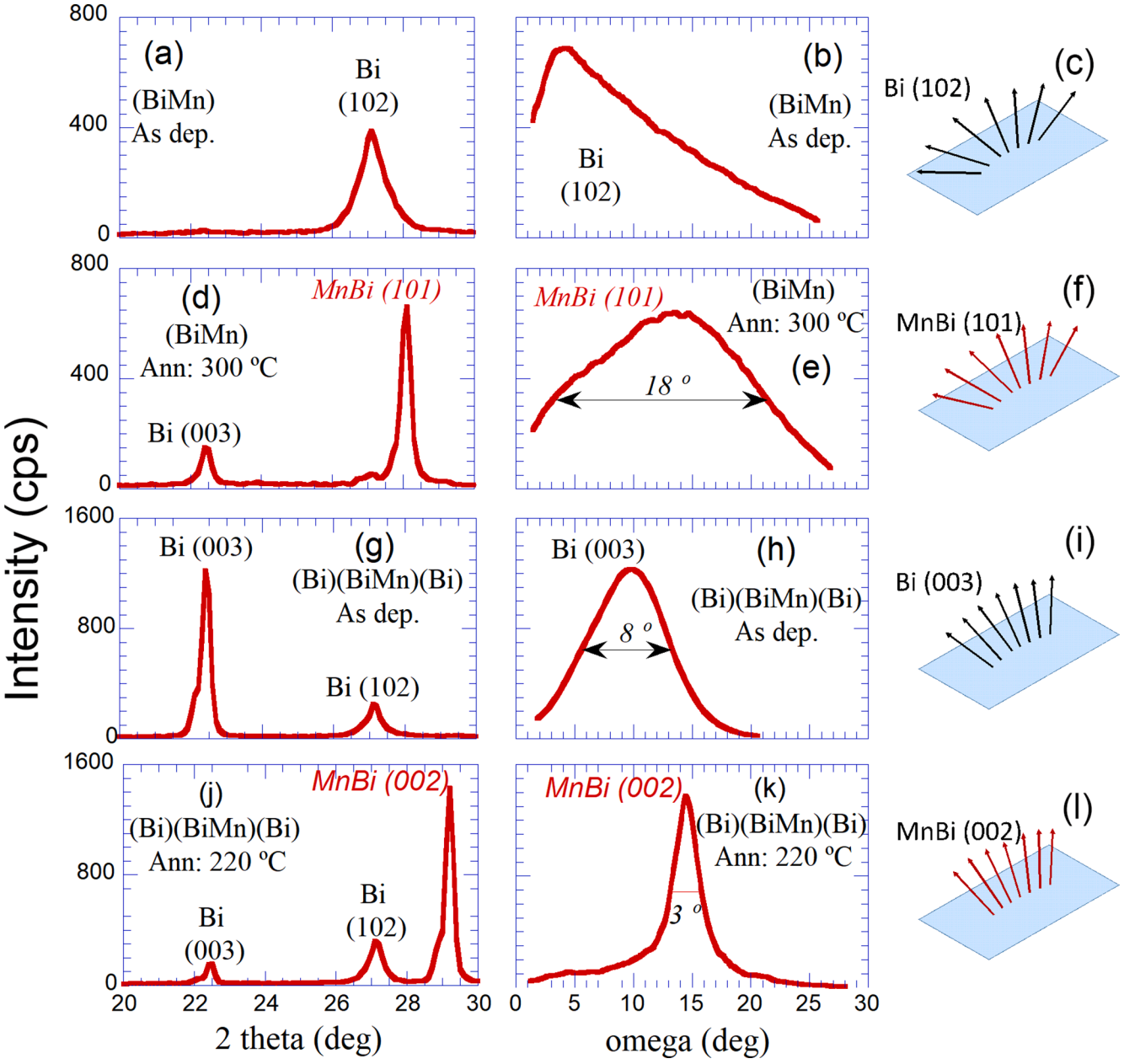

Fig. 4. X-ray diffraction pattern of the as deposited and annealed $(Bi_{3.2nm}Mn_{1.4nm})_{40}$ (a), (d) and $Bi_{50nm}/(Bi_{3.2nm}Mn_{1.4nm})_{40}/Bi_{50nm}$ samples (g), (j), respectively. Rocking curves of the selected peaks of the as deposited and annealed $(Bi_{3.2nm}Mn_{1.4nm})_{40}$ (b), (e) and $Bi_{50nm}/(Bi_{3.2nm}Mn_{1.4nm})_{40}/Bi_{50nm}$ samples (h), (k), respectively. Schematic drawings of the crystallites distributions of the previous samples (c), (f), (i), (l).

magnetization in this sample could be due to a displacement of a domain wall. This fact would be consistent with the decrease of the coercivity measured in this sample. Several works reported in the scientific literature also detailed a reduction of the coercivity of the MnBi films when a preferential orientation perpendicular to the film plane was observed [6,7,8,11].

Thus, from the previous magnetic measurements, the most significant characteristic of the sample with extra Bi layers was that MnBi grains grew with a preferential orientation, different from what was found in the samples without the Bi buffer and capping layer. Therefore, in order to confirm this evidence from a structural viewpoint, we have performed rocking curve measurements around some particular diffraction peaks of the different samples. In this way, Fig. 4(a) represents the X-ray diffraction pattern of the as deposited $(Bi_{3.2nm}Mn_{1.4nm})_{40}$ sample where only the main Bi (1 0 2) peak was observed. The rocking curve around this peak, cf. Fig. 4(b) displays a broad maximum that could correspond to the instrumental response, rather than to a preferential growth of the Bi grains. A picture of the distribution of Bi grains from the previous measurements is represented in Fig. 4(c). On annealing this sample, LT-MnBi phase grew and the MnBi (1 0 1) peak was observed in the corresponding diffraction diagram (Fig. 4(d)). A rocking curve around this peak, Fig. 4(e) also showed a broad maximum which indicated a slight texture of the MnBi grains. The absence of a strong texture in the MnBi grains was thus consistent with the magnetic measurements on this sample, showing only a weak anisotropy perpendicular to the film plane. Also a schematic drawing of the orientation of the MnBi grains was shown in Fig. 4(f).

On the other side, the X-ray diffraction pattern of the as deposited $Bi_{50nm}/(Bi_{3.2nm}Mn_{1.4nm})_{40}/Bi_{50nm}$ film displayed a strong Bi (0 0 3) peak, cf. Fig. 4(g). The rocking curve performed around this Bi (0 0 3) peak, Fig. 4(h), showed a sharper maximum, that confirmed the preferential growth of Bi with the c-axis perpendicular to the film plane. The drawing in Fig. 4(i) indicates this preferential growth. Thus it seems reasonable to assume that Bi growth with a preferential orientation could serve as a template for the further growth of MnBi grains upon annealing. Consequently, Fig. 4(j) displays the X-ray diffraction pattern of the $Bi_{50nm}/(Bi_{3.2nm}Mn_{1.4nm})_{40}/Bi_{50nm}$ film annealed at 220 °C, where the MnBi (0 0 2) was observed. A rocking curve measurement around this peak, cf. Fig. 4(k), confirmed the assumed preferential growth of the MnBi grains by showing a sharp maximum (FWHM = 3°) around an omega angle of 14.6°. Again, the picture in Fig. 4(l) indicated the preferential growth of the MnBi grains with their c-axes in the perpendicular direction.

It is worth pointing out that in this $Bi_{50nm}/(Bi_{3.2nm}Mn_{1.4nm})_{40}/Bi_{50nm}/Ta_{15nm}$ sample the temperature of the formation of the MnBi phase was considerably reduced (by more than 50 °C) with respect to what was observed in the $(Bi_{3.2nm}Mn_{1.4nm})_{40}/Ta_{15nm}$ sample. Furthermore, this reduction was even larger (by roughly 120 °C) when compared to previous samples [16] with lower relative content of Bi in the film. The mechanism responsible for the formation of the MnBi phase at different temperatures, could be the diffusion of Mn and Bi atoms throughout the samples upon annealing. The diffusion coefficient of both Mn and Bi is governed by an activation mechanism described by an Arrhenius law. In this respect, the activation energy roughly depends on the melting temperature. Since the melting temperature of Bi is 544 K, and the melting temperature of Mn is 1521 K, the diffusion coefficient at the typical annealing temperatures described in this manuscript is much larger for Bi than for Mn. Thus, in this case, the diffusion constant for Bi at the annealing temperature range could be around $10^{-13}\ m^2\ s^{-1}$, while the diffusion coefficient for Mn in the same temperature range could be $10^{-25}\ m^2\ s^{-1}$ [27]. It could thus be reasonable to assume that on increasing the Bi concentration, the diffusion of atoms to generate the LT-MnBi phase would increase. Consequently, the formation of the MnBi phase in our samples could take place at lower temperatures.

4. Discussion

The influence of the environment on the structure, magnetic domain configuration and magnetic properties of MnBi samples was manifested through the previous results. Thus, X-ray diffraction pattern of the $(Bi_{3.2nm}Mn_{1.4nm})_{40}/Ta_{15nm}$ films displayed a polycrystalline structure where approximately the c-axis of the MnBi grains pointed in random directions. Since the magnetization of MnBi was along the c-axis direction, the magnetization of the previous samples was close to isotropic. Only a small preferential growth of the MnBi crystallites in the sample anneaded at 300 °C, in the perpendicular to the plane direction seemed to originate the slight difference between the hysteresis loops measured with the applied magnetic field either perpendicular or parallel to the film plane. In this $(Bi_{3.2nm}Mn_{1.4nm})_{40}/Ta_{15nm}$ sample, the magnetization was correlated to the structure of the films. Thus Fig. 5(a) shows the AFM images of a similar film annealed at 330 °C. The presence of MnBi grains, whose size is in the micron range was evidenced in the topographic image. Fig. 5(b), (c) and (d) show the MFM images that corresponded to different magnetic states of the film:

- the sample in a negative remanent state after the application of a magnetic field of −1.7 T perpendicular to the film plane (Fig. 5(b)),
- the sample in the demagnetized state (Fig. 5(c)),
- and the sample in a positive remanent state after the application of a magnetic field of 1.7 T, perpendicular to the film plane (Fig. 5(d)).

These MFM images display the presence of magnetic domains through bright and dark regions whose size was in average around 2 μm. Both in the topographic image as well as in the magnetic images we have highlighted the magnetic state corresponding to two MnBi grains (particles 1 and 2 in Fig. 5). Their size, from the topographic image, was also around 2 μm. These two particles displayed different domain configurations depending on the macroscopic magnetic state of the sample. Nevertheless, these different domain configurations within the particles were restricted to the volume of every particle, which suggested that the magnetic state of the particles was directly correlated to the particle's morphology. It would be reasonable to assume that these MnBi particles that constitute the sample, could behave like weakly interacting particles, since the almost random distribution of their easy magnetization directions as well as the high value of the uniaxial anisotropy energy, Ku ($\approx 10^6\ J/m^3$) [23], could prevent their coupling via a direct exchange interaction.

The AFM images of the $Mn_{20nm}/(Bi_{3.2n\mu}Mn_{1.4nm})_{40}/Mn_{20nm}/Ta_{15nm}$ film annealed at 260 °C, are shown in Fig. 6(a) and 6(c) meanwhile the MFM images for the same sample are displayed in Fig. 6(b) and 6(d). In this sample, the correlation between the structure of the MnBi grains and their magnetism was not direct. Thus, grains with a broad distribution of sizes between 400 nm and 4 μm were observed in the AFM images. Magnetic domains, whose size is far beyond the micron size, do not seem to be correlated with most of the grains observed in the AFM images. However, some correlation may be observed between one particle on the bottom of Fig. 6 (a) (highlighted with a circle) that has a corresponding magnetic domain in Fig. 6 (b). Also, a large particle (whose size was roughly 5 μm, highlighted with a circle, too) was clearly observed in Fig. 6 (c). This particle originated a strong magnetic contrast (see Fig. 6 (d)) corresponding to a particle's magnetic moment on the film plane. Nevertheless, in spite of the former correspondences, the correlation between structure and magnetic domain configuration was progressively lost in this sample.

In the $Bi_{50nm}/(Bi_{3.2nm}Mn_{1.4nm})_{40}/Bi_{50nm}/Ta_{15nm}$ film, no correlation at all, between topography (cf. Fig. 7 (a)) and magnetism (cf. Fig. 7 (b)) could be found in the sample annealed at 220 °C. This lack of direct correlation between topography and magnetism was also found in the magnetic domain structure of $SmCo_5$ magnets [28]. The MFM image on the 220 °C annealed sample displayed a multidomain structure where the magnetization pointed either upwards or downwards. In this

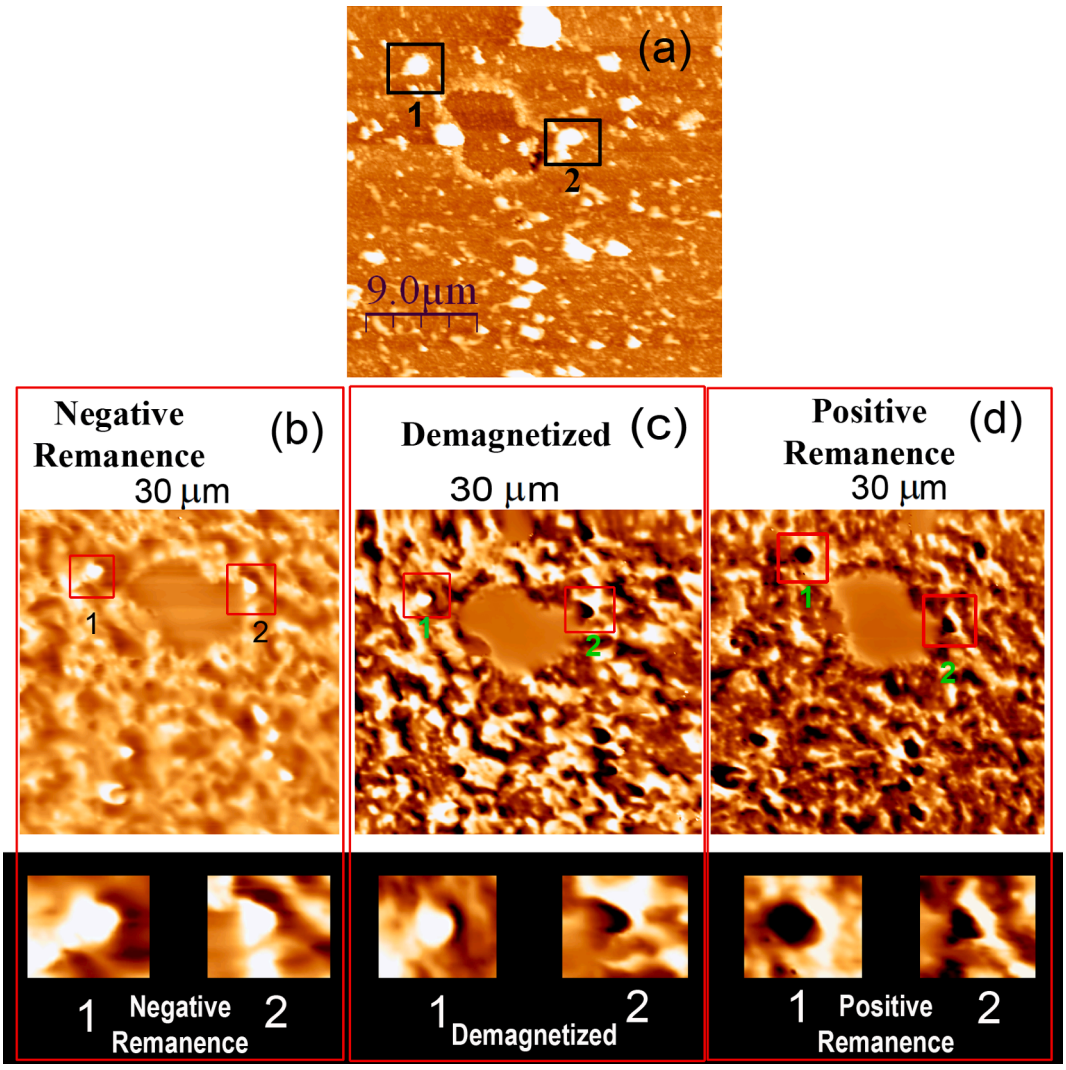

Fig. 5. 30 * 30 μm^2 AFM (a) and MFM (b), (c) and (d), images of a (Bi/Mn) film that was annealed at 330 °C in different magnetic states. The topography and the magnetic domain configuration of particles 1 and 2 are highlighted in the figure.

situation it would be reasonable to assume that the magnetic moments of the different MnBi grains with their c-axes parallel, could be coupled by the exchange interaction, leading to large perpendicular magnetic domains. In other words, the exchange coupling between the MnBi grains would be favored by the parallel alignment of the c-axes of the MnBi grains. The reversal of the magnetization in this sample would take place by displacement of domain walls and consequently a decrease in the coercivity of the sample would be observed.

A similar behavior of the coercivity was reported in MnBi alloys obtained by the suction casting technique [29,30]. In that case, the as cast sample consisted on a mixture of different phases, pure Mn, pure Bi and MnBi where the size of the different regions was on the order of several (2–6) μm. The coercivity, on the order of 0.3 T, was assumed to be due to a nucleation process. However, the coercivity decreased roughly one order of magnitude upon increasing the size of the MnBi regions, beyond the tens of microns, due to annealing. The mechanism for the coercivity in these annealed samples was the pinning mechanism.

5. Conclusion

MnBi films fabricated upon annealing PLD $(Bi_{3.2nm}Mn_{1.4nm})_{40}$ films displayed hard magnetic properties with saturation magnetization on the order of 450 emu/cm^3 and coercivity around 1 Tesla. The annealed samples displayed a MnBi polycristalline structure with a random distribution of the c-axes of the MnBi grains, giving rise to an almost isotropic magnetization. Magnetic domains whose size was in the range between 1 and 2 μm, associated to the presence of MnBi grains, were observed in the MFM image.

When Mn was added to the previous sample as buffer and capping layers, $Mn_{20nm}/(Bi_{3.2nm}Mn_{1.4nm})_{40}/Mn_{20nm}$, the macroscopic properties of the annealed sample did not change, compared to the sample without extra Mn layers: the almost isotropic saturation magnetization was also 450 emu/cm^3 and the coercivity around 1 Tesla. The X-ray diffraction pattern of this sample also showed a MnBi polycristalline structure. However, for this sample the size of the magnetic domains were larger than those in the sample without the extra Mn layer and larger than most of the grains observed on the surface of the film. However still some correlation between the magnetization and granular structure was found on this Mn rich sample. In some grains whose size was in the range from 2 to 4 μm, magnetic domains confined to the volume of the particles were found.

On the contrary, when adding extra Bi buffer and capping layers a preferential orientation of the MnBi grains, perpendicular to the film plane, was observed through rocking curve measurements. This fact gave rise to the observation of an out-of-plane easy magnetization direction. The magnetic hysteresis loops corresponding to the annealed samples were clearly anisotropic. Although the saturation magnetization of the sample was 500 emu/cm^3, the value of the coercivity

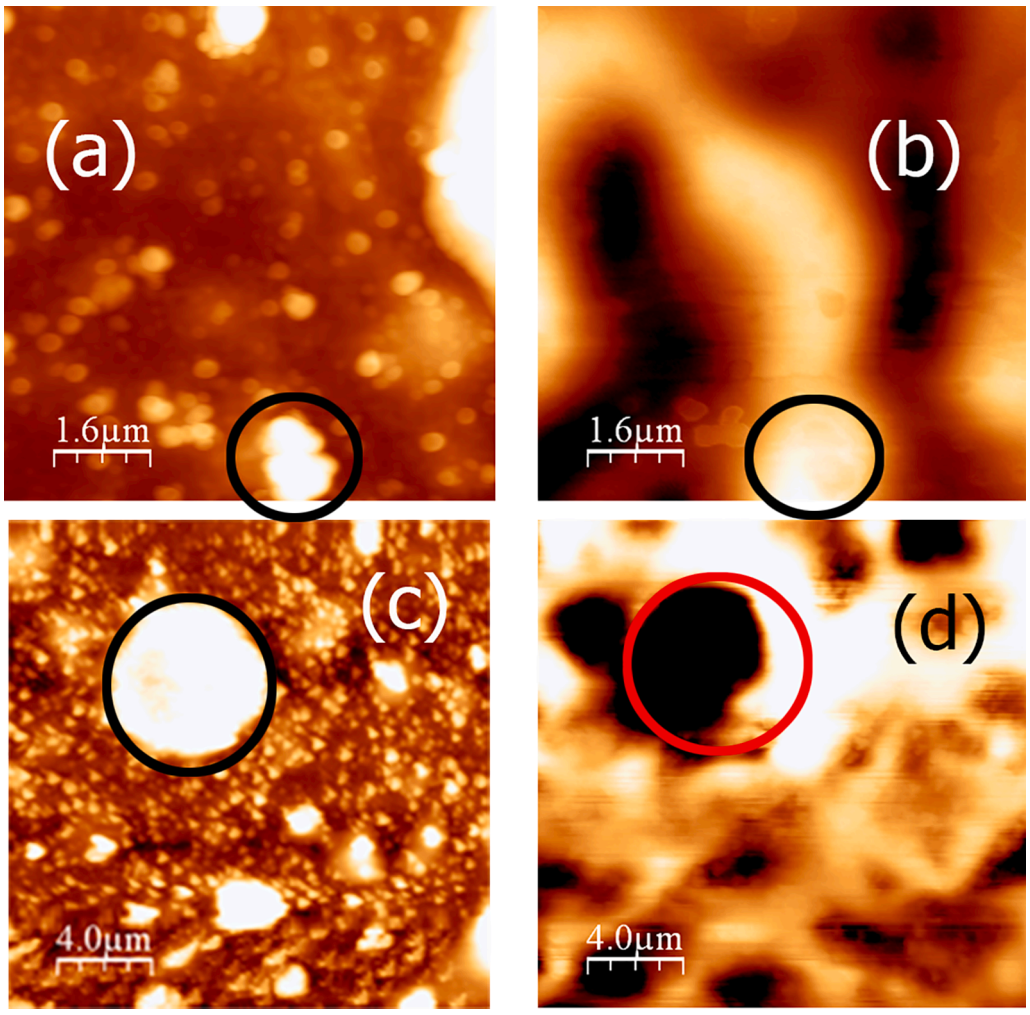

Fig. 6. AFM (a), (c) and MFM (b), (d), images of the $Mn_{20nm}/(Bi_{3.2nm}Mn_{1.4nm})_{40}/ Mn_{20nm}/Ta_{15nm}$ annealed at 260 °C. The circles in the images highlight the presence of MnBi grains along with their magnetic domain configuration.

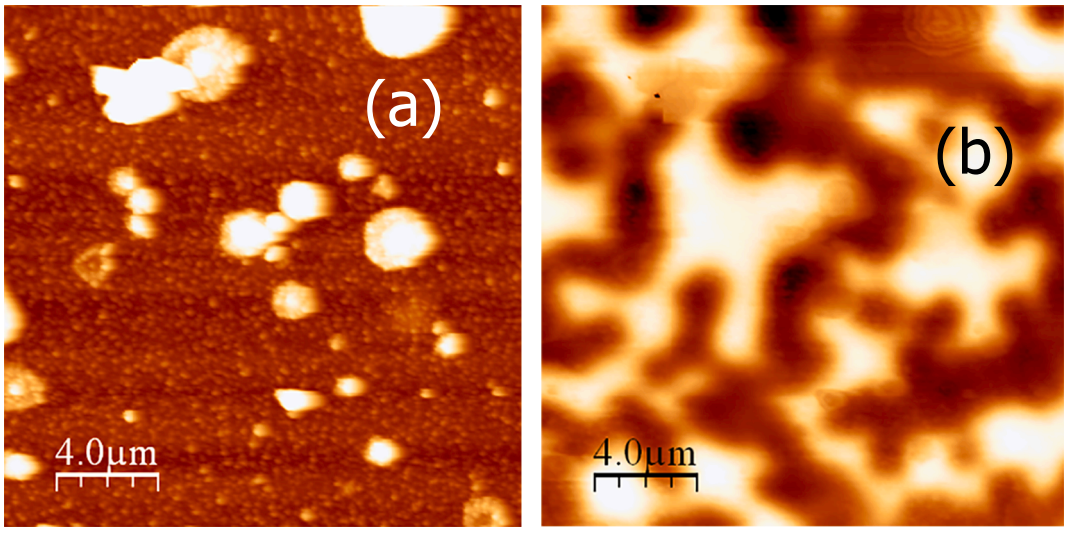

Fig. 7. AFM (a) and MFM (b), images of the $Bi_{50nm}/(Bi_{3.2nm}Mn_{1.4nm})_{40}/Bi_{50nm}/Ta_{15nm}$ annealed at 220 °C.

decreased significantly (around one order of magnitude with respect to the coercivity measured in the previous samples without extra Bi layers). In this case, the magnetic moments of the different MnBi grains could be exchanged coupled since their easy magnetization directions were parallel. This fact could be on the basis of the formation of large magnetic domains, uncorrelated with the particular MnBi grains. The

magnetization reversal in this sample could take place by domain wall motion, giving rise to the observed decrease in the coercivity of the MnBi sample with extra Bi layers.

CRediT authorship contribution statement

J. Vergara: Conceptualization, Investigation, Methodology, Formal analysis, Writing – original draft, Writing – review & editing, Visualization. **C. Favieres:** Conceptualization, Investigation, Methodology, Formal analysis, Writing – review & editing. **V. Madurga:** Conceptualization, Investigation, Methodology, Formal analysis, Writing – review & editing.

Declaration of Competing Interest

The authors declare that they have no known competing financial interests or personal relationships that could have appeared to influence the work reported in this paper.

Acknowledgements

The authors acknowledge the partial finantial support from Universidad Pública de Navarra and from Gobierno de España. Open access funding by Universidad Pública de Navarra.

References

[1] D. Li, D.S. Pan, S.J. Li, Z.D. Zhang, Recent developments of rare –earth –free hard-magnetic materials, Sci. China-Phys. Mech. Astron. 59 (2016), 617501, https://doi.org/10.1007/s11433-015-5760-x.
[2] X. Guo, X. Chen, Z. Altounian, J.O. Ström-Olsen, Magnetic properties of MnBi prepared by rapid solidification, Phys. Rev. B 46 (22) (1992) 14578–14582, https://doi.org/10.1103/PhysRevB.46.14578.
[3] B.W. Roberts, Neutron diffraction study of the structures and magnetic properties of manganese bismuthide, Phys. Rev. 104 (3) (1956) 607–616, https://doi.org/10.1103/PhysRev.104.607.
[4] T. Hozumi, P. LeClair, G. Mankey, C. Mewes, H. Sepehri-Amin, K. Hono, T. Suzuki, Magnetic and structural properties of MnBi multilayered thin film, J. Appl. Phys. 115 (2014) 17A737, https://doi.org/10.1063/1.4867127.
[5] M. Ito, Y. Tanaka, T. Satoh, G. Mankey, R. Schad, T. Suzuki, Magnetic properties and structure of low temperature phase MnBi with island structure, AIP Adv. 7 (5) (2017) 056226, https://doi.org/10.1063/1.4977230.
[6] S. Sabet, E. Hildebrandt, F.M. Römer, I. Radulov, H. Zhang, M. Farle, L. Alff, Low-temperature phase c-axis oriented manganese bismuth thin films with high anisotropy grown from an alloy $Mn_{55}Bi_{45}$ target, IEEE Trans. Magn. 53 (2017) 2100306, https://doi.org/10.1109/TMAG.2016.2636817.
[7] H. Moon, S. Kim, H. Jung, H.-S. Lee, W. Lee, Layer-number dependence of the magnetic properties of MnBi films, Appl. Surf. Sci. 420 (2017) 618–624, https://doi.org/10.1016/j.apsusc.2017.05.149.
[8] E. Céspedes, M. Villanueva, C. Navío, F.J. Mompeán, M. García-Hernández, A. Inchausti, P. Pedraz, M.R. Osorio, J. Camarero, A. Bollero, High coercive LTP-MnBi for high temperature applications: From isolated particles to film-like structures, J. Alloy. Comp. 729 (2017) 1156–1164, https://doi.org/10.1016/j.jallcom.2017.09.234.
[9] P. Quarterman, D. Zhang, K.B. Schliep, T.J. Peterson, Y. Lv, J.-P. Wang, Effect of capping layer on formation and magnetic properties of MnBi thin films, J. Appl. Phys. 122 (21) (2017) 213904, https://doi.org/10.1063/1.5001081.
[10] M.Y. Sun, X.W. Xu, X.A. Liang, X.W. Sun, Y.J. Zheng, Effect of oxidation on perpendicular magnetic behavior of MnBi thin films, J. Alloy. Comp. 672 (2016) 59–63, https://doi.org/10.1016/j.jallcom.2016.01.240.
[11] V.G. Myagkov, L.E. Bykova, V.Y. Yakovchuk, A.A. Matsynin, D.A. Velikanov, G. S. Patrin, G.Y. Yurkin, G.N. Bondarenko, High rotatable magnetic anisotropy in MnBi thin films, JETP Lett. 105 (10) (2017) 651–656, https://doi.org/10.1134/S0021364017100095.
[12] W. Zhang, P. Kharel, S. Valloppilly, L. Yue, D.J. Sellmyer, High-energy-product MnBi films with controllable anisotropy, Phys. Status Solidi B 252 (9) (2015) 1934–1939.
[13] P. Kharel, X.Z. Li, V.R. Shah, N. Al-Aqtash, K. Tarawneh, R.F. Sabirianov, R. Skomski, D.J. Sellmyer, Structural, magnetic and electron transport properties of MnBi: Fe thin films, J. Appl. Phys. 111 (7) (2012) 07E326, https://doi.org/10.1063/1.3675615.
[14] D. Zhou, Y.F. Zhang, X.B. Ma, S.Q. Liu, J.Z. Han, M.G. Zhu, C.S. Wang, J.B. Yang, Preparation of highly textured Bi and MnBi films by Pulser Laser Deposition method, Chin. Phys. Lett. 32 (2015), 127502, https://doi.org/10.1088/0256-307X/32/12/127502.
[15] Y.F. Zhang, J.Z. Han, S.Q. Liu, H.D. Tian, H. Zhao, H.L. Du, Y.C. Yang, Y.K. Fang, W. Li, J.B. Yang, Structural modification and ultra-high coercivity of nanostructural anisotropic MnBi/Bi films, Acta Mater. 128 (2017) 96–102, https://doi.org/10.1016/j.actamat.2017.02.012.
[16] J. Vergara, C. Favieres, V. Madurga, MnBi hard magnetic films optimized through the correlation between resistivity, morphology and magnetic properties, J. Magn. Magn. Mater. 491 (2019), 165525, https://doi.org/10.1016/j.jmmm.2019.165525.
[17] W. Liu, Z. Zhang, Anisotropic nanocomposite soft/hard multilayer magnets, Chin. Phys. B 26 (2017), https://doi.org/10.1088/1674-1056/26/11/117502.
[18] B. Li, W. Liu, X.G. Zhao, W.J. Gong, X.T. Zhao, H.L. Wang, D. Kim, C.J. Choi, Z. D. Zhang, The structural and magnetic properties of MnBi and exchange coupled MnBi/Fe films, J. Magn. Magn. Mater. 372 (2014) 12–15, https://doi.org/10.1016/j.jmmm.2014.07.027.
[19] S. Sabet, E. Hildebrandt, L. Alff, Synthesis and magnetic properties of the thin film exchange spring system of MnBi/FeCo, J. Phys. Conf. Ser. 903 (2017) 012032, https://doi.org/10.1088/1742-6596/903/1/012032.
[20] Y. Yan, J. Guo, J. Li, R. Li, Magnetically exchange coupled MnBi/FeCo thin film composites with enhanced maximum energy products, Mater. Lett. 184 (2016) 13–16, https://doi.org/10.1016/j.matlet.2016.08.015.
[21] S. Sabet, A. Moradabadi, S. Gorji, M. Yi, Q. Gong, M.H. Fawey, E. Hildebrandt, D. Wang, H. Zhang, B.-X. Xu, C. Kübel, L. Alff, Impact of interface structure on magnetic exchange coupling in MnBi/Fe_xCo_{1-x} bilayers, Phys. Rev. B 98 (2018), 174440, https://doi.org/10.1103/PhysRevB.98.174440.
[22] D. Chen, Perparation and stability of MnBi thin films, J. Appl. Phys. 42 (1971) 3625–3628, https://doi.org/10.1063/1.1660779.
[23] V.N. Antonov, V.P. Antropov, Low-temperature MnBi alloys: Electronic and magnetic properties, constitution, morphology and fabrication, Low Temp. Phys. 46 (2020), 000000, https://doi.org/10.1063/10.0000360.
[24] V. Madurga, J. Vergara, C. Favieres, Influence of the nature of the substrate on the soft magnetic properties of pulsed laser ablated-deposited amorphous Co, J. Magn. Magn. Mater. 254–255 (2003) 140–142, https://doi.org/10.1016/s0304-8853(02)00808-9.
[25] I. Horcas, R. Fernández, J.M. Gómez-Rodríguez, J. Colchero, J. Gómez-Herrero, A. M. Baró, WSXM: A software for scanning probe microscopy and a tool for nanotechnology, Rev. Sci. Instrum. 78 (2007) 0137, https://doi.org/10.1063/1.2432410.
[26] G. Ciuta, F. Dumas-Bouchiat, N.M. Dempsey, O. Fruchart, Some aspects of Magnetic Force Microscopy of Hard Magnetic Films, IEEE Trans. Magn. 52 (9) (2016) 1–8, https://doi.org/10.1109/TMAG.2016.2558642.
[27] H. Mehrer, Diffusion in Solids, Springer Ser. Solid-State Sci. (2007). https://doi:10.1007/978-3-540-71488-0.
[28] W. Szmaja, J. Grobelny, M. Cichomski, Domain structure of sintered $SmCo_5$ magnets studied by magnetic force microscopy, Appl. Phys. Lett. 85 (14) (2004) 2878–2880, https://doi.org/10.1063/1.1801165.
[29] J. Zamora, I. Betancourt, I.A. Figueroa, Switching of Coercivity Process in MnBi Alloys, J. Supercon. Nov. Mang. 31 (3) (2018) 873–878, https://doi.org/10.1007/s10948-017-4240-0.
[30] J. Zamora, I. Betancourt, I.A. Figueroa, Coercivity mechanism of rare-earth free MnBi hard magnetic alloys, Rev. Mex. Fís. 64 (2018) 141–144, https://doi.org/10.31349/RevMexFis.64.141.